

Cyclic Functional Mapping: Self-supervised correspondence between non-isometric deformable shapes

Dvir Ginzburg
Tel Aviv University
dvirginzburg@mail.tau.ac.il

Dan Raviv
Tel Aviv University
darav@tauex.tau.ac.il

Abstract

We present the first utterly self-supervised network for dense correspondence mapping between non-isometric shapes. The task of alignment in non-Euclidean domains is one of the most fundamental and crucial problems in computer vision. As 3D scanners can generate highly complex and dense models, the mission of finding dense mappings between those models is vital. The novelty of our solution is based on a cyclic mapping between metric spaces, where the distance between a pair of points should remain invariant after the full cycle. As the same learnable rules that generate the point-wise descriptors apply in both directions, the network learns invariant structures without any labels while coping with non-isometric deformations. We show here state-of-the-art-results by a large margin for a variety of tasks compared to known self-supervised and supervised methods.

1. Introduction

Alignment of non-rigid shapes is a fundamental problem in computer vision and plays an important role in multiple applications such as pose transfer, cross-shape texture mapping, 3D body scanning, and simultaneous localization and mapping (SLAM). The task of finding dense correspondence is especially challenging for non-rigid shapes, as the number of variables needed to define the mapping is vast, and local deformations might occur. To this end, we have seen a variety of papers focusing on defining unique key-points. These features capture the local uniqueness of the models using curvature [30], normals [40], or heat [37], for example, and further exploited for finding a dense mapping [13, 5].

A different approach used for alignment is based on pairwise distortions, where angles [6, 23] or distances [16, 9] between pairs of points are minimized. Formulating this as

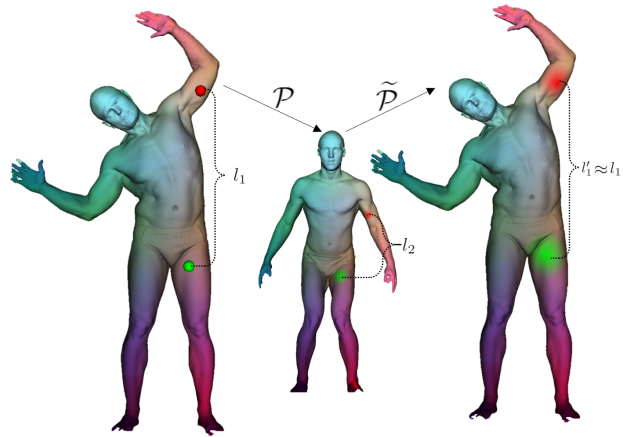


Figure 1: Self-supervised dense correspondence using a cycle mapping architecture. By minimizing the geodesic distortion only on the source shape, we can learn complex deformations between structures.

a linear [44] or quadratic [9, 39, 2] optimization scheme showed a significant enhancement but with a painful time complexity even for small models.

To confront the challenges in alignment between stretchable shapes we recognize non-metric methods based on conformal mapping [23], experimenting with alternative metrics such as scale [4] or affine invariant metrics [31], or attempts to embed the shapes into a plane or a cone [12, 10], for example. A significant milestone named functional maps [29] has shown that such a mapping can be performed on the spectral domain, by aligning functions overlaid on top of the shapes.

Recently, a substantial improvement in dense alignment emerged using data-driven solutions, where axiomatic shape models and deformations were replaced by learnable counterparts. Among those methods a highly successfully research direction was based on learning local features overlaid on the vertices of the shapes [24], where ResNet [20]

like architecture is used to update SHOT descriptors [40].

The main challenge new data-driven geometric alignment algorithms need to face is the lack of data to train on or labeled data used for supervised learning. In many cases, the labeled data is expensive to generate or even infeasible to acquire, as seen, for example, in medical imaging.

A recent approach [19] showed that self-supervised learning could be applied for non-rigid alignment between isometric shapes by preserving the pair-wise distance measured on the source and on the target. While showing good results, an isometric limitation is a strong constraint that is irrelevant in many scenarios. On a different note, self-supervised learning was recently addressed in images, where a cyclic mapping between pictures, known as cyclic-GAN, was introduced [45, 27, 43]. The authors showed that given unpaired collection of images from different domains, a cyclic-loss that measures the distortion achieves robust state-of-the-art results in unsupervised learning for domain transfer.

In this work, we claim that one can learn dense correspondence in a self-supervised manner in between non-isometric structures. We present a new learnable cyclic mechanism, where the same model is used both for forward and backward mapping learning to compensate for deformed parts. We measure the pair-wise distance distortion of the cyclic mapping on randomly chosen pair of points only from the source manifold. We show here state-of-the-art-results by a large margin for a variety of tasks compared to self-supervised and supervised methods, in isometric and non-isometric setups.

2. Contribution

We present an unsupervised learning scheme for dense 3D correspondence between shapes, based on learnable self similarities between metric spaces. The proposed approach has multiple advantages over other known methods. First, there is no need to define a model for the shapes or the deformations; Second, no need for labeled data with dense correspondence mappings. Third, the proposed method can handle isometric or non-isometric deformations and partial matching. The cyclic mapping approach allows our system to learn the geometric representation of manifolds by feeding it pairs of matching shapes, even without any labels, by measuring a geometric criterion (pair-wise distance) only on the source.

Our main contribution is based on the understanding that a cyclic mapping between metric spaces which follows the same rules, forces the network to learn invariant parts. We built the cyclic mapping using the functional maps frame-

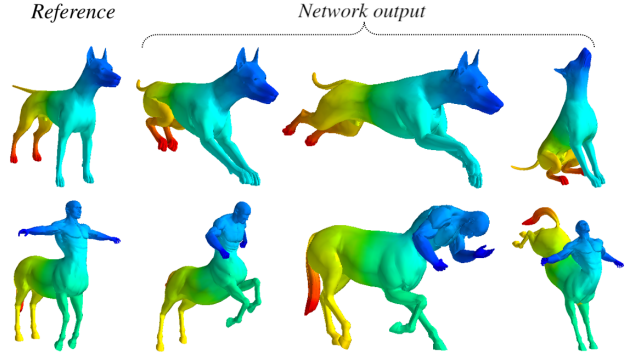


Figure 2: TOSCA dataset results - similar colors represents correspondence mapping - we show excellent generalization after training for a single epoch on the TOSCA dataset with a pre-trained model on FAUST 6.5

work [29], optimizing for a soft correspondence between shapes on the spectral domains by updating a local descriptor per point. The proposed approach can be adapted to any dimension, and here we provide state-of-the-art results on surfaces. We show results that are comparable to supervised learning [24, 18, 22] methods in the rare case we possess dense correspondence labels, and outperforms self-supervised learning approaches [18, 19] when the shapes are isometric. Once the deformations are not isometric, our method stands out, and outperforms other methods by a large margin.

3. Background

Our cyclic mapping is built on top of functional maps architecture. To explain the foundations of this approach, we must elaborate on distance matrices, functional maps and how to weave deep learning into functional maps. Finally, we discuss an isometric unsupervised approach for the alignment task and its limitations, which motivated this work.

3.1. Riemannian 2-manifolds

We model 3D shapes as a Riemannian 2-manifold (\mathcal{X}, g) , where \mathcal{X} is a real smooth manifold, equipped with an inner product g_p on the tangent space $T_p\mathcal{X}$ at each point p that varies smoothly from point to point in the sense that if \mathcal{U} and \mathcal{V} are differentiable vector fields on \mathcal{X} , then $p \rightarrow g_p(\mathcal{U}|_p, \mathcal{V}|_p)$ is a smooth function.

We equip the manifolds with a distance function $d_{\mathcal{X}} : \mathcal{X} \times \mathcal{X} \rightarrow \mathbb{R}$ induced by the standard volume form $d\mathcal{X}$. We state the distance matrix $\mathcal{D}_{\mathcal{X}}$, as a square symmetric matrix, represents the manifold’s distance function $d_{\mathcal{X}}$ such that

$$\mathcal{D}_{\mathcal{X}ij} = d_{\mathcal{X}}(X_i, X_j)$$

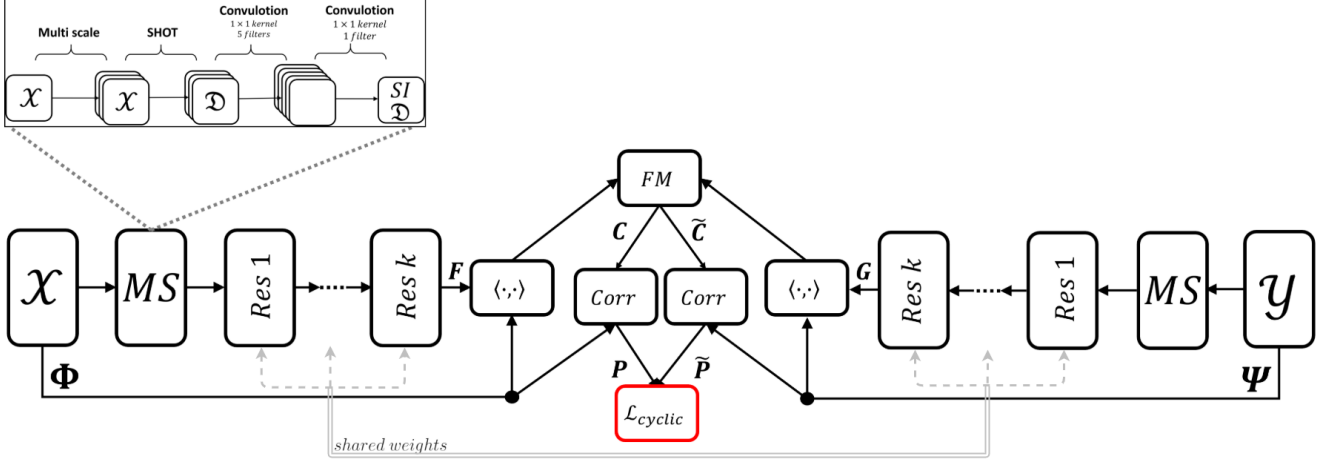


Figure 3: Cyclic functional mapper in between two manifolds \mathcal{X} and \mathcal{Y} (left and right sides). The multi-scaled descriptors (top left, marked MS) based on shot [40] are passed to a ResNet like network, resulting in two corresponding coefficient matrices F and G . By projecting the refined descriptors onto the spectral space, two mappings, C and \tilde{C} , are computed. The two soft correspondence matrices P and \tilde{P} are further used as part of the network cyclic loss \mathcal{L}_{cyclic} as shown in equation 9.

3.2. Functional maps

Functional maps [29] stands for matching real-valued functions in between manifolds instead of performing a straight forward point matching. Using a spectral basis, one can extract a compact representation for a match on the spectral domain. The clear advantage here is that many natural constraints on the map become linear constraints on the functional map. Given two manifolds \mathcal{X} and \mathcal{Y} , and functional spaces on top $F(\mathcal{X})$ and $F(\mathcal{Y})$, we can define a functional map using orthogonal bases ϕ and ψ

$$\begin{aligned} Tf &= T \sum_{i \geq 1} \langle f, \phi_i \rangle_{\mathcal{Y}} \phi_i = \sum_{i \geq 1} \langle f, \phi_i \rangle_{\mathcal{Y}} T \phi_i \\ &= \sum_{i, j \geq 1} \langle f, \phi_i \rangle_{\mathcal{Y}} \underbrace{\langle T \phi_i, \psi_j \rangle_{\mathcal{X}}}_{c_{ij}} \psi_j, \end{aligned} \quad (1)$$

where $C \in \mathbb{R}^{k \times k}$ represents the mapping in between the domains given k matched functions, and every pair of corresponding functions on-top of the manifolds impose a linear constraint on the mapping. The coefficient matrix C is deeply depended on the choice of the bases ϕ, ψ , and as shown in prior works [29, 32, 19] a good choice for such bases is the Laplacian eigenfunctions of the shapes.

3.3. Deep functional maps

Deep functional maps were first introduced in [24], where the mapping C in between shapes was refined by learning new local features per point. The authors showed that using a ResNet [20] like architecture on-top of SHOT

[40] descriptors, they can revise the local features in such a way that the global mapping is more accurate. The mapping is presented as a soft correspondence matrix P where P_{ji} is the probability \mathcal{X}_i corresponds to \mathcal{Y}_j . The loss of the network is based on geodesic distortion between the corresponding mapping and the ground truth, reading

$$\mathcal{L}_{sup}(\mathcal{X}, \mathcal{Y}) = \frac{1}{|\mathcal{X}|} \left\| \left(P \circ (\mathcal{D}_{\mathcal{Y}} \Pi^*) \right) \right\|_F^2, \quad (2)$$

where $|\mathcal{X}|$ is the number of vertices of shape \mathcal{X} , and if $|\mathcal{X}| = n$, and $|\mathcal{Y}| = m$, then $\Pi^* \in \mathbb{R}^{m \times n}$ is the ground-truth mapping between \mathcal{X} and \mathcal{Y} , $\mathcal{D}_{\mathcal{Y}} \in \mathbb{R}^{m \times m}$ is the geodesic distance matrix of \mathcal{Y} , \circ denote a point-wise multiplication, and $\|_F$ is the Frobenius norm. For each target vertex, the loss penalizes by the distance between the actual corresponding vertex and the assumed one, multiplied by the amount of certainty the network has in that correspondence. Hence the loss is zero if

$$P_{ji} = 1 \Leftrightarrow \Pi^*(\mathcal{X}_i) = \mathcal{Y}_j$$

as $\mathcal{D}(y, y) = 0 \forall y \in \mathcal{Y}$.

3.4. Self-supervised deep functional maps

The main drawback of deep functional maps is the need for ground truth labels. Obtaining alignment maps for domains such as ours is a strong requirement, and is infeasible in many cases either due to the cost to generate those datasets, or even impractical to collect. In a recent paper [19], the authors showed that for isometric deformations,

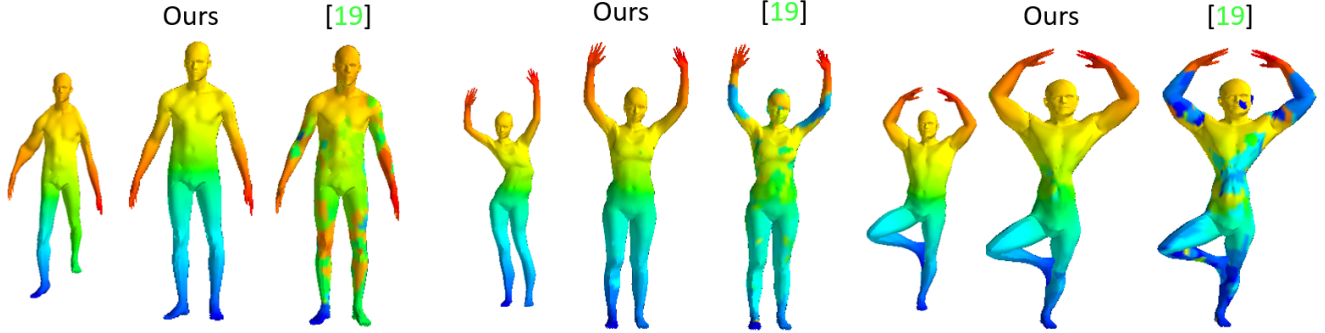


Figure 4: Alignment between non-isometric shapes, where similar parts appear in similar colors. The shapes were locally scaled and stretched while changing their pose. Our approach learns the correct matching while [19] fails under local stretching.

we can replace the ground truth requirement with a different geometric criterion based on pair-wise distances. In practice, they married together the Gromov-Hausdorff framework with the deep functional maps architecture.

The Gromov-Hausdorff distance which measures the distance in between metric spaces, reads

$$d_{GH}(\mathcal{X}, \mathcal{Y}) = \frac{1}{2} \inf_{\pi} (dis(\pi)), \quad (3)$$

where the infimum is taken over all correspondence distortions of a given mapping $\pi: \mathcal{X} \mapsto \mathcal{Y}$. This distortion can be translated to a pair-wise distance [16, 21] notation, which was used by [19] as a geometric criterion in the cost function of a deep functional map setup. Unfortunately, the pair-wise distance constraint is an extreme demand, forcing the models to be isometric, and can not be fulfilled in many practical scenarios.

4. Cyclic self-supervised deep functional maps

The main contribution of this paper is the transition from the pair-wise distance comparison between source and target manifolds to a method that only examines the metric in the source manifold. Every pair of distances are mapped to the target and re-mapped back to the source. We use the same model for the forward and backward mapping to avoid a mode collapse, and we measure the distortion once a cyclic map has been completed, forcing the model to learn how to compensate for the deformations.

4.1. Correspondence distortion

A mapping $\pi: M \rightarrow N$ between two manifolds generates a pair-wise distortion

$$dis_{\pi}(\mathcal{X}, \mathcal{Y}) = \sum_{x_1, x_2 \in \mathcal{X}} \rho(d_{\mathcal{X}}(x_1, x_2), d_{\mathcal{Y}}(\pi(x_1), \pi(x_2))), \quad (4)$$

where ρ is usually an L_p norm metric, and $p = 2$ is a useful choice of the parameter.

As isometric mapping preserves pair-wise distances, minimizing the distances between those pairs provides a good metric-dependent correspondence. Specifically,

$$\pi^{iso}(\mathcal{X}, \mathcal{Y}) = \operatorname{argmin}_{\pi: \mathcal{X} \rightarrow \mathcal{Y}} dis_{\pi}(\mathcal{X}, \mathcal{Y}). \quad (5)$$

Solving 5 takes the form of a quadratic assignment problem. The main drawback of this criterion, as the name suggests, is the isometric assumption. While it is a powerful tool for isometric mappings, natural phenomena do not follow that convention as stretching exists in the data. To overcome those limitations, we present here the cyclic distortion criterion.

4.2. Cyclic distortion

We define a **cyclic distortion** π^{cyc} as a composition of two mappings $\pi_{\rightarrow}: \mathcal{X} \rightarrow \mathcal{Y}$ and $\pi_{\leftarrow}: \mathcal{Y} \rightarrow \mathcal{X}$, which leads to a cyclic distortion

$$dis_{(\pi_{\rightarrow}, \pi_{\leftarrow})}^{cyc}(\mathcal{X}, \mathcal{Y}) = \sum_{x_1, x_2 \in \mathcal{X}} \rho(d_{\mathcal{X}}(x_1, x_2), d_{\mathcal{X}}(\tilde{x}_1, \tilde{x}_2)), \quad (6)$$

where $\tilde{x}_1 = \pi_{\leftarrow}(\pi_{\rightarrow}(x_1))$ and $\tilde{x}_2 = \pi_{\leftarrow}(\pi_{\rightarrow}(x_2))$.

π_{\rightarrow} and π_{\leftarrow} are being optimized using the same sub-network, implemented as shared weights in the learning process. Every forward mapping π_{\rightarrow} induce a backward mapping π_{\leftarrow} and vice-versa. We call this coupled pair $\pi = (\pi_{\rightarrow}, \pi_{\leftarrow})$ a *conjugate mapping*, and denote the space of all conjugate mappings by \mathcal{S} . We define the cyclic mapping as

$$\pi^{cyc}(\mathcal{X}, \mathcal{Y}) = \operatorname{argmin}_{\pi: (\mathcal{X} \rightarrow \mathcal{Y}, \mathcal{Y} \rightarrow \mathcal{X}) \in \mathcal{S}} dis_{\pi}^{cyc}(\mathcal{X}, \mathcal{Y}). \quad (7)$$

4.3. Deep cyclic mapping

Following the functional map convention, given C, Φ, Ψ the *soft correspondence matrix* mapping between \mathcal{X} to \mathcal{Y} reads [24]

$$P = |\Phi C \Psi^T|_{\mathcal{F}_c}, \quad (8)$$

where each entry P_{ji} is the probability point j in \mathcal{X} corresponds to point i in \mathcal{Y} . We further use $|\cdot|_{\mathcal{F}_c}$ notation for column normalization, to emphasize the statistical interpretation of P .

Let P represents the forward mapping π_{\rightarrow} soft correspondence and \tilde{P} the backward mapping π_{\leftarrow} . The cyclic distortion is defined by

$$\mathcal{L}_{cyclic}(\mathcal{X}, \mathcal{Y}) = \frac{1}{|\mathcal{X}|^2} \left\| \left(D_{\mathcal{X}} - (\tilde{P}P) D_{\mathcal{X}} (\tilde{P}P)^T \right) \right\|_{\mathcal{F}}^2, \quad (9)$$

where $|\mathcal{X}|$ is the number of samples point pairs on \mathcal{X} .

Note that if we assumed the shapes were isometric, then we would have expected $D_{\mathcal{Y}}$ to be similar or even identical to $P D_{\mathcal{X}} P^T$, which yields once plugged into (9) the isometric constraint

$$\mathcal{L}_{isometric}(\mathcal{X}, \mathcal{Y}) = \frac{1}{|\mathcal{X}|^2} \left\| \left(D_{\mathcal{X}} - \tilde{P} D_{\mathcal{Y}} \tilde{P}^T \right) \right\|_{\mathcal{F}}^2. \quad (10)$$

The cyclic distortion (9) is self-supervised, as no labels are required, and only use the pair-wise distances on the source manifold \mathcal{X} . The conjugate mappings are based on the functional maps architecture and use the geometry of both spaces, source and target. Since we constraint the mapping on the source’s geometry, the mapping copes with stretching, and thus learning invariant representations.

5. Implementation

5.1. Hardware

The network was developed in TensorFlow [1], running on a GeForce GTX 2080 Ti GPU. The SHOT descriptor [40] was implemented in MATLAB, while the Laplace Beltrami Operator (LBO) [34] and geodesic distances were calculated in Python.

5.2. Pre-processing

We apply a sub-sampling process for shapes with more than 10,000 points using qSlim [17] algorithm. SHOT descriptor was computed on the sub-sampled shapes, generating a descriptor of length $s = 350$ per vertex. Finally,

Method	Scans		Synthetic	
	inter	intra	inter	intra
Ours	4.068	2.12	2.327	2.112
Litany <i>et al.</i> [24]	4.826	2.436	2.452	2.125
Halimi <i>et al.</i> [19]	4.883	2.51	3.632	2.213
Groueix <i>et al.</i> [18]	4.833	2.789	—	—
Li <i>et al.</i> [22]	4.079	2.161	—	—
Chen <i>et al.</i> [14]	8.304	4.86	—	—

Table 1: Average error on the FAUST dataset measured as distance between mapped points and the ground truth. We compared between our approach and other supervised and unsupervised methods.



Figure 5: Correspondence on FAUST real scans dataset, where similar colors represent the same correspondence. This dataset contains shapes made of $\sim 100k$ vertices with missing information in various poses. We use a post-matching PMF filter [42], and show qualitative results in Table 1. We outperform both supervised and unsupervised methods.

the LBO eigenfunctions corresponding to the least significant 70 eigenvalues were computed for each shape. The distance matrices were computed using the Fast Marching algorithm [35]. In order to initialize the conjugate mapping, we found that a hard constraint on P and \tilde{P} coupling provides good results. Specifically we minimized in the first epoch the cost function $\|P\tilde{P} - I\|_{\mathcal{F}}^2$ before applying the soft cyclic criterion (9).

5.3. Network architecture

The architecture is motivated by [24, 19] and shown in Figure 3. The input to the first layer is the raw 3D triangular mesh representations of the two figures given by a list of vertices and faces. We apply a multi-layer SHOT [40] descriptor by evaluating the SHOT on $m \sim 5$ global scaled versions of the input. The figures vary from 0.2 to 2 times the size of the original figures, followed by a 1×1 convolution layers with $2m$ filters, to a 1×1 convolution layer with one filter, generating an output of $n \times s$ descriptor to the network. Besides, the relevant eigenfunctions and pair-wise distance matrix of the source shape are provided as parameters to the network.

The next stage is the ResNet [20] layers with the shared weights applied to both figures. Subsequently, the non-linear descriptors are multiplied by the $n \times k$ LBO eigenfunctions. We calculate the forward and backward mappings C and \tilde{C} using the same network and evaluate the corresponding forward and backward mappings P and \tilde{P} , which are fed into the soft cyclic loss (9).

6. Experiments

In this section, we present multiple experiments in different settings; synthetic and real layouts, transfer learning tasks, non-isometric transformations, partial matching and one-shot learning. We show benchmarks, as well as comparisons to state-of-the-art solutions, both for axiomatic and learned algorithms.

6.1. Mesh error evaluation

The measure of error for the correspondence mapping between two shapes will be according to the Princeton benchmark [21], that is, given a mapping $\pi_{\rightarrow}(\mathcal{X}, \mathcal{Y})$ and the ground truth $\pi_{\rightarrow}^*(\mathcal{X}, \mathcal{Y})$ the error of the correspondence matrix is the sum of geodesic distances between the mappings for each point in the source figure, divided by the area of the target figure.

$$\epsilon(\pi_{\rightarrow}) = \sum_{x \in \mathcal{X}} \frac{\mathcal{D}_{\mathcal{Y}}(\pi_{\rightarrow}(x), \pi_{\rightarrow}^*(x))}{\sqrt{\text{area}(\mathcal{Y})}}, \quad (11)$$

where the approximation of $\text{area}(\bullet)$ for a triangular mesh is the sum of its triangles area.

6.2. Synthetic FAUST

We compared our alignment on FAUST dataset [7] versus supervised [24] and unsupervised [19] methods. We followed the experiment as described in [24] and used the synthetic human shapes dataset, where the first 80 shapes (8 subjects with 10 different poses each) are devoted to training, and 20 shapes made of 2 different unseen subjects are used for testing. For a fair comparison between methods, we did not run the PMF cleanup filter [42] as this procedure is extremely slow and takes about 15 minutes for one shape build of $\sim 7k$ vertices on an i9 desktop.

We do not perform any triangular mesh preprocessing on the dataset, that is, we learn on the full resolution of 6890 vertices. Each mini-batch is of size 4 (i.e 4 pairs of figures), using $k = 120$ eigenfunctions, and 10 bins in SHOT with a radius set to be 5% of the geodesic distance from each vertex.

We report superior results for inter-subject and intra-subject tasks in Table 1, while converging faster (see Figure 6).

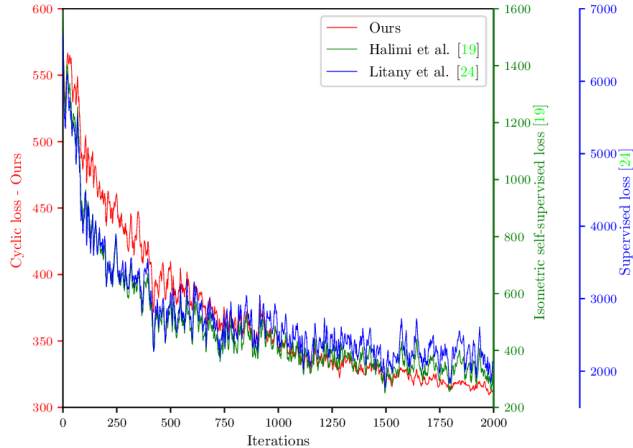


Figure 6: We visualize our cyclic loss, the isometric constrained unsupervised loss [19], and the supervised loss [24] during the training of our cyclic loss on the synthetic FAUST dataset. We show that minimization of the cyclic loss on isometric structures is equivalent (after normalization) to minimizing the isometric constraint or applying ground truth labels to the learning.

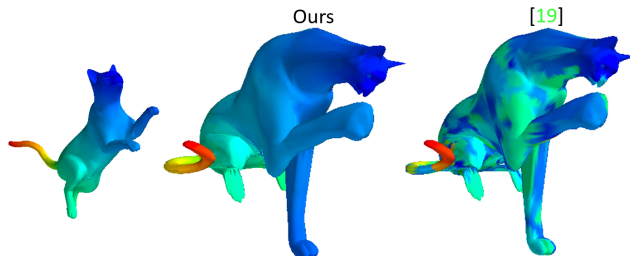


Figure 7: Single pair (one shot) learning on deformable non-isometric shapes. Supervised methods as [24] are irrelevant, where isometric self-learning approach fails [19].

6.3. Real scans

We tested our method on real 3D scans of humans from the FAUST [7] dataset. While the synthetic samples had $\sim 6k$ vertices, each figure in this set has $\sim 150k$ vertices, creating the amount of plausible cyclic mappings extremely high. The dataset consists of multiple subjects in a variety of poses, where none of the poses (e.g., women with her hands up) in the test set were present in the training set. The samples were acquired using a full-body 3D stereo capture system, resulting in missing vertices, and open-end meshes. The dataset is split into two test cases as before, the intra and inter subjects (60 and 40 pairs respectively), and ground-truth correspondences in not given. Hence, the geodesic error evaluation is provided as an online service. As suggested in [24], after evaluating the soft correspon-

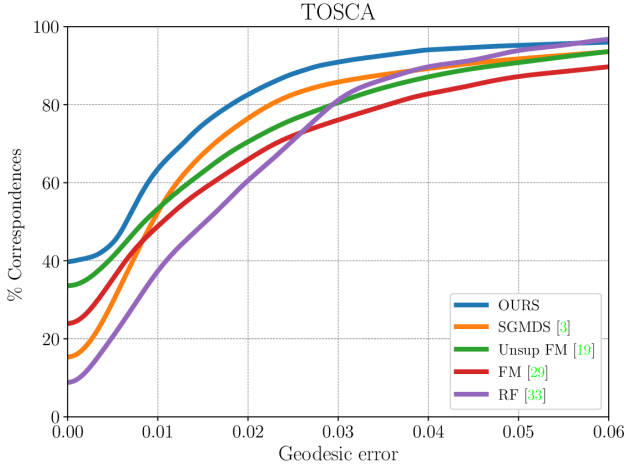


Figure 8: Geodesic error on TOSCA dataset. We report superior results against other supervised and unsupervised learnable methods. Note that the compared methods did not run a post-processing optimization-based filter, or received partial matching as input.

dence mappings, we input our map to the PMF algorithm [42] for a smoother bijective correspondence refined map. We report state of the art results on both inter and intra class mappings in comparison to all the unsupervised techniques. We provide visualization in Figure 5 and qualitative results in table 1.

6.4. Non-isometric deformations

An even bigger advantage of the proposed method is its ability to cope with local stretching. Due to the cyclic mapping approach, we learn local matching features directly between the models and are not relying on a base shape in the latent space or assume isometric consistency. We experimented with models generated in Autodesk Maya that were locally stretched and bent. We show visual results in Figure 4. The proposed approach successfully handle large non-isometric deformations.

6.5. TOSCA

The TOSCA dataset [11] consists of 80 objects from different domains as animals and humans in different poses. Although the animals are remarkably different in terms of LBO decomposition, as well as geometric characteristics, our model achieves excellent performance in terms of a geodesic error on the dataset after training for a single epoch on it, using the pre-trained model from the real scans FAUST dataset.

In Figure 8, we show a comparison between our and other supervised and unsupervised approaches and visual-

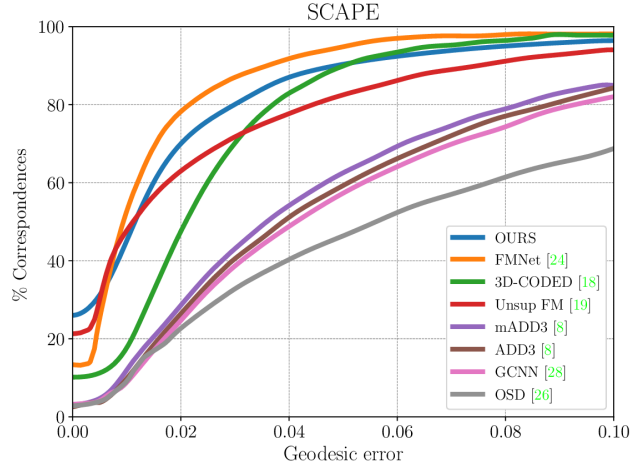


Figure 9: Geodesic error on SCAPE dataset. Our network was trained on FAUST dataset and used to predict the mapping on SCAPE. We provide superior results on all unsupervised and almost all supervised methods showing good generalization properties.

ize a few samples in Figure 2. Compared methods results were taken from [19]. Our network was trained for a single epoch on the dataset, with a pre-trained model of the real scans FAUST data and yet, shows great performance. We report state of the art results, compared to axiomatic, supervised, and unsupervised methods. Also note that while other methods mention training on each class separately, we achieve state-of-the-art results while training jointly.

6.6. SCAPE

To further emphasize the generalization capabilities of our network, we present our results on the SCAPE dataset [38], which is an artificial human shape dataset, digitally generated, with completely different properties from the FAUST dataset in any aspect (geometric entities, scale, ratio, for example). Nevertheless, our network that was trained on the real scan FAUST dataset performs remarkably well. See Figure 9. Compared methods results were taken from [19].

6.7. One-shot single pair learning

Following the experiment shown in [19], we demonstrate that we can map in between two shapes seen for the first time without training on a large dataset. Compared to optimization approaches we witness improved running time due to optimized hardware and software dedicated to deep learning in recent years. In Figure 7 we show such a mapping in between highly deformed shapes, and we found it intriguing that a learning method based on just two sam-

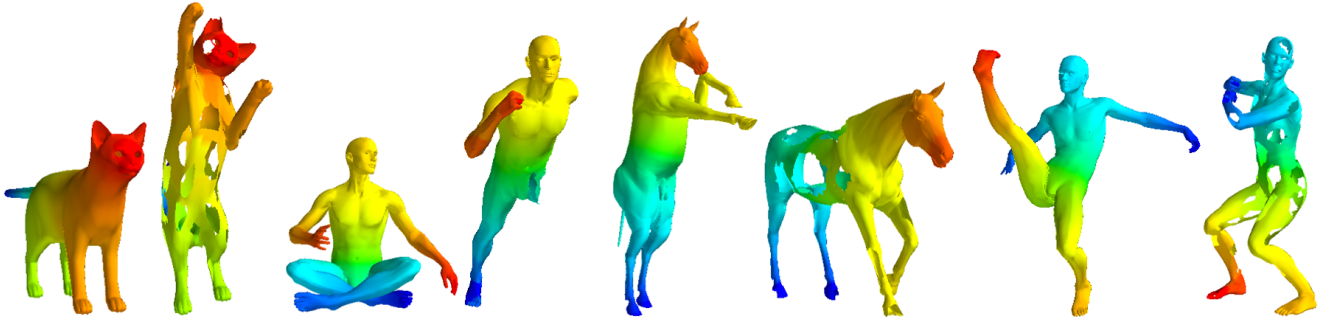


Figure 10: Partial shapes correspondence on SHREC 16 [15] dataset after removing substantial parts (upto 75%). In every pair, we mapped the left shape into the right one, where similar mapped points share the color. Our method is robust to missing information.

ples can converge to a feasible solution even without strong geometric assumptions. Note that in that case methods based on isometric criterion fail to converge due to the large non-isometric deformation. In this experiment we used our multi-SHOT pre-trained weights before we ran our cyclic mapper.

6.8. Partial shapes correspondence

The partial shapes correspondence task is inherently more complicated than the full figure alignment problems. While in most experiments shown above, the number of vertices in both shapes differed by less than 5%, in the partial shapes task, we consider mappings between objects that differ by a large margin of up to 75% in their vertex count. To this end, numerous bijective solutions, such as [36, 41, 42] show degraded performance on the partial challenge, resulting in targeted algorithms [32, 25] for the mission. With that in mind, we show our results on the SHREC 2016 [15] partial shapes dataset. We use the same architecture as described earlier, given hyperparameters and trained weights from the TOSCA 6.5 experiment, showing our network’s generalization capabilities. As before, we have trained the network on this dataset only for a single epoch.

7. Limitations

Our method uses functional maps architecture, which requires us to pre-compute sets of bases functions. To that end, this process can not be done in real-time in the current setup, and there might be an inconsistency in bases functions between shapes due to noise or large non-isometric deformations. While this method works well for isometric or stretchable domains, once the deformations are significantly large, we found that the current system does not converge to a reasonable geodesic error in terms of a pleasant visual so-

lution, which makes it challenging to use in cross-domain alignments. We believe that the proposed approach can be used as part of semantic-correspondence to overcome those limitations.

8. Summary

We presented here a cyclic architecture for dense correspondence between shapes. This approach is self-supervised, can cope with local stretching as well as non-rigid isometric deformations. It outperforms other unsupervised and supervised approaches on tested examples, and we report state-of-the-art results in several scenarios, including real 3D scans and partial matching task.

References

- [1] Martín Abadi, Ashish Agarwal, Paul Barham, Eugene Brevdo, Zhifeng Chen, Craig Citro, Greg S. Corrado, Andy Davis, Jeffrey Dean, Matthieu Devin, Sanjay Ghemawat, Ian Goodfellow, Andrew Harp, Geoffrey Irving, Michael Isard, Yangqing Jia, Rafal Jozefowicz, Lukasz Kaiser, Manjunath Kudlur, Josh Levenberg, Dan Mané, Rajat Monga, Sherry Moore, Derek Murray, Chris Olah, Mike Schuster, Jonathon Shlens, Benoit Steiner, Ilya Sutskever, Kunal Talwar, Paul Tucker, Vincent Vanhoucke, Vijay Vasudevan, Fernanda Viégas, Oriol Vinyals, Pete Warden, Martin Wattenberg, Martin Wicke, Yuan Yu, and Xiaoqiang Zheng. TensorFlow: Large-Scale Machine Learning on Heterogeneous Systems, 2015. Software available from tensorflow.org. [5](#)
- [2] Yonathan Aflalo, Alexander Bronstein, and Ron Kimmel. On convex relaxation of graph isomorphism. *Proceedings of the National Academy of Sciences*, 112(10):2942–2947, 2015. [1](#)
- [3] Yonathan Aflalo, Anastasia Dubrovina, and Ron Kimmel. Spectral Generalized Multi-dimensional Scaling. *International Journal of Computer Vision*, 118(3):380–392, 2016.
- [4] Yonathan Aflalo, Ron Kimmel, and Dan Raviv. Scale invariant geometry for nonrigid shapes. *SIAM Journal on Imaging Sciences*, 6(3):1579–1597, 2013. [1](#)
- [5] Mathieu Aubry, Ulrich Schlickewei, and Daniel Cremers. The wave kernel signature: A quantum mechanical approach to shape analysis. In *2011 IEEE international conference on computer vision workshops (ICCV workshops)*, pages 1626–1633. IEEE, 2011. [1](#)
- [6] Mirela Ben-Chen, Craig Gotsman, and Guy Bunin. Conformal Flattening by Curvature Prescription and Metric Scaling. In *Computer Graphics Forum*, volume 27, pages 449–458. Wiley Online Library, 2008. [1](#)
- [7] Federica Bogo, Javier Romero, Matthew Loper, and Michael J. Black. FAUST: Dataset and evaluation for 3D mesh registration. In *Proceedings IEEE Conf. on Computer Vision and Pattern Recognition (CVPR)*, Piscataway, NJ, USA, June 2014. IEEE. [6](#)
- [8] Davide Boscaïni, Jonathan Masci, Emanuele Rodolà, Michael M. Bronstein, and Daniel Cremers. Anisotropic Diffusion Descriptors. *Comput. Graph. Forum*, 35:431–441, 2016.
- [9] Alexander M Bronstein, Michael M Bronstein, and Ron Kimmel. Generalized multidimensional scaling: a framework for isometry-invariant partial surface matching. *Proceedings of the National Academy of Sciences*, 103(5):1168–1172, 2006. [1](#)
- [10] Alexander M Bronstein, Michael M Bronstein, and Ron Kimmel. Generalized multidimensional scaling: A framework for isometry-invariant partial surface matching. *Proceedings of the National Academy of Sciences*, 103(5):1168–1172, 2006. [1](#)
- [11] Alexander M Bronstein, Michael M Bronstein, and Ron Kimmel. *Numerical geometry of non-rigid shapes*. Springer Science & Business Media, 2008. [7](#)
- [12] Michael M Bronstein, Alexander M Bronstein, Ron Kimmel, and Irad Yavneh. Multigrid multidimensional scaling. *Numerical linear algebra with applications*, 13(2-3):149–171, 2006. [1](#)
- [13] Michael M Bronstein and Iasonas Kokkinos. Scale-invariant heat kernel signatures for non-rigid shape recognition. In *2010 IEEE Computer Society Conference on Computer Vision and Pattern Recognition*, pages 1704–1711. IEEE, 2010. [1](#)
- [14] Qifeng Chen and Vladlen Koltun. Robust Nonrigid Registration by Convex Optimization. In *Proceedings of the IEEE International Conference on Computer Vision*, pages 2039–2047, 2015. [5](#)
- [15] Luca Cosmo, Emanuele Rodolà, Michael M Bronstein, Andrea Torsello, Daniel Cremers, and Y Sahillioglu. SHREC16: Partial matching of deformable shapes. [8](#)
- [16] Asi Elad and Ron Kimmel. On bending invariant signatures for surfaces. *IEEE Transactions on pattern analysis and machine intelligence*, 25(10):1285–1295, 2003. [1, 4](#)
- [17] Michael Garland and Paul S Heckbert. Surface simplification using quadric error metrics. In *Proceedings of the 24th annual conference on Computer graphics and interactive techniques*, pages 209–216. ACM Press/Addison-Wesley Publishing Co., 1997. [5](#)
- [18] Thibaut Groueix, Matthew Fisher, Vladimir G. Kim, Bryan C. Russell, and Mathieu Aubry. 3D-CODED : 3D Correspondences by Deep Deformation. *CoRR*, abs/1806.05228, 2018. [2, 5](#)
- [19] Oshri Halimi, Or Litany, Emanuele Rodola, Alex M Bronstein, and Ron Kimmel. Unsupervised Learning of Dense Shape Correspondence. In *Proceedings of the IEEE Conference on Computer Vision and Pattern Recognition*, pages 4370–4379, 2019. [2, 3, 4, 5, 6, 7](#)
- [20] Kaiming He, Xiangyu Zhang, Shaoqing Ren, and Jian Sun. Deep Residual Learning for Image Recognition. *CoRR*, abs/1512.03385, 2015. [1, 3, 6](#)
- [21] Vladimir G Kim, Yaron Lipman, and Thomas Funkhouser. Blended intrinsic maps. In *ACM Transactions on Graphics (TOG)*, volume 30, page 79. ACM, 2011. [4, 6](#)
- [22] Chun-Liang Li, Tomas Simon, Jason Saragih, Barnabás Póczos, and Yaser Sheikh. LBS Autoencoder: Self-supervised Fitting of Articulated Meshes to Point Clouds. In *Proceedings of the IEEE Conference on Computer Vision and Pattern Recognition*, pages 11967–11976, 2019. [2, 5](#)
- [23] Yaron Lipman and Ingrid Daubechies. Conformal Wasserstein distances: Comparing surfaces in polynomial time. *Advances in Mathematics*, 227(3):1047–1077, 2011. [1](#)
- [24] Or Litany, Tal Remez, Emanuele Rodolà, Alexander M. Bronstein, and Michael M. Bronstein. Deep Functional Maps: Structured prediction for dense shape correspondence. *CoRR*, abs/1704.08686, 2017. [1, 2, 3, 5, 6](#)
- [25] Or Litany, Emanuele Rodolà, Alexander M Bronstein, and Michael M Bronstein. Fully Spectral Partial Shape Match-

- ing. In *Computer Graphics Forum*, volume 36, pages 247–258. Wiley Online Library, 2017. [8](#)
- [26] Roei Litman and Alexander M Bronstein. Learning spectral descriptors for deformable shape correspondence. *IEEE transactions on pattern analysis and machine intelligence*, 36(1):171–180, 2013.
- [27] Ming-Yu Liu, Thomas Breuel, and Jan Kautz. Unsupervised Image-to-Image Translation Networks. In *Advances in neural information processing systems*, pages 700–708, 2017. [2](#)
- [28] Jonathan Masci, Davide Boscaini, Michael Bronstein, and Pierre Vandergheynst. Geodesic convolutional neural networks on Riemannian manifolds. In *Proceedings of the IEEE international conference on computer vision workshops*, pages 37–45, 2015.
- [29] Maks Ovsjanikov, Mirela Ben-Chen, Justin Solomon, Adrian Butscher, and Leonidas Guibas. Functional maps: a flexible representation of maps between shapes. *ACM Transactions on Graphics (TOG)*, 31(4):30, 2012. [1](#), [2](#), [3](#)
- [30] Helmut Pottmann, Johannes Wallner, Qi-Xing Huang, and Yong-Liang Yang. Integral Invariants for Robust Geometry Processing. *Computer Aided Geometric Design*, 26(1):37–60, 2009. [1](#)
- [31] Dan Raviv, Michael M Bronstein, Alexander M Bronstein, Ron Kimmel, and Nir Sochen. Affine-invariant diffusion geometry for the analysis of deformable 3d shapes. In *CVPR 2011*, pages 2361–2367. IEEE, 2011. [1](#)
- [32] Emanuele Rodolà, Luca Cosmo, Michael M Bronstein, Andrea Torsello, and Daniel Cremers. Partial functional correspondence. In *Computer Graphics Forum*, volume 36, pages 222–236. Wiley Online Library, 2017. [3](#), [8](#)
- [33] Emanuele Rodolà, Samuel Rota Bulo, Thomas Windheuser, Matthias Vestner, and Daniel Cremers. Dense Non-Rigid Shape Correspondence using Random Forests. In *Proceedings of the IEEE Conference on Computer Vision and Pattern Recognition*, pages 4177–4184, 2014.
- [34] Raif M. Rustamov. Laplace-beltrami eigenfunctions for deformation invariant shape representation. In *Proceedings of the Fifth Eurographics Symposium on Geometry Processing, SGP '07*, pages 225–233, Aire-la-Ville, Switzerland, Switzerland, 2007. Eurographics Association. [5](#)
- [35] James A Sethian. A fast marching level set method for monotonically advancing fronts. *Proceedings of the National Academy of Sciences*, 93(4):1591–1595, 1996. [5](#)
- [36] Jonathan Starck and Adrian Hilton. Spherical Matching for Temporal Correspondence of Non-Rigid Surfaces. In *Tenth IEEE International Conference on Computer Vision (ICCV'05) Volume 1*, volume 2, pages 1387–1394. IEEE, 2005. [8](#)
- [37] Jian Sun, Maks Ovsjanikov, and Leonidas Guibas. A Concise and Provably Informative Multi-Scale Signature Based on Heat Diffusion. In *Computer graphics forum*, volume 28, pages 1383–1392. Wiley Online Library, 2009. [1](#)
- [38] Richard Szeliski, Dragomir Anguelov, Praveen Srinivasan, Daphne Koller, Sebastian Thrun, Jim Rodgers, and James Davis. *SCAPE: shape completion and animation of people*, volume 24. 2005. [7](#)
- [39] Art Tevs, Alexander Berner, Michael Wand, Ivo Ihrke, and H-P Seidel. Intrinsic shape matching by planned landmark sampling. In *Computer Graphics Forum*, volume 30, pages 543–552. Wiley Online Library, 2011. [1](#)
- [40] Federico Tombari, Samuele Salti, and Luigi Di Stefano. Unique Signatures of Histograms for Local Surface Description. In *Computer Vision – ECCV 2010*, pages 356–369, 2010. [1](#), [2](#), [3](#), [5](#)
- [41] Matthias Vestner, Zorah Löhner, Amit Boyarski, Or Litany, Ron Slossberg, Tal Remez, Emanuele Rodola, Alex Bronstein, Michael Bronstein, Ron Kimmel, et al. Efficient deformable shape correspondence via kernel matching. In *2017 International Conference on 3D Vision (3DV)*, pages 517–526. IEEE, 2017. [8](#)
- [42] Matthias Vestner, Roei Litman, Emanuele Rodolà, Alex Bronstein, and Daniel Cremers. Product manifold filter: Non-rigid shape correspondence via kernel density estimation in the product space. In *Proceedings of the IEEE Conference on Computer Vision and Pattern Recognition*, pages 3327–3336, 2017. [5](#), [6](#), [7](#), [8](#)
- [43] Zili Yi, Hao Zhang, Ping Tan, and Minglun Gong. Dual-GAN: Unsupervised dual learning for Image-to-Image translation. In *Proceedings of the IEEE international conference on computer vision*, pages 2849–2857, 2017. [2](#)
- [44] Andrei Zaharescu, Edmond Boyer, Kiran Varanasi, and Radu Horaud. Surface Feature Detection and Description with Applications to Mesh Matching. In *2009 IEEE Conference on Computer Vision and Pattern Recognition*, pages 373–380. IEEE, 2009. [1](#)
- [45] Jun-Yan Zhu, Taesung Park, Phillip Isola, and Alexei A Efros. Unpaired Image-to-Image Translation using Cycle-Consistent Adversarial Networks. In *Proceedings of the IEEE international conference on computer vision*, pages 2223–2232, 2017. [2](#)